ISSN 0016-8521, Geotectonics, 2020, Vol. 54, No. 6, pp. 821–831. © Pleiades Publishing, Inc., 2020.

Paleostress Analysis from Fractures in Kalosh Anticline, Kurdistan Region, North–East of Iraq

S. H. Sulaiman Al-Hakari[a, *], O. Tokmachi[b], and A. Abdalla[b]

[a] *University of Sulaymani, Geology Department, College of Science, Sulaimani, 46001 Iraq*

[b] *Kirkuk University, Applied Geology Department, College of Science, Kirkuk, 36001 Iraq*

**e-mail: salim.sulaiman@univsul.edu.iq*

Received April 24, 2019; revised June 6, 2020; accepted July 28, 2020

Abstract—Fractures analysis carried out throughout traverses across Kalosh anticline. The anticline is located ~30 km south of Sulaimaniyah city, Kurdistan region, NE Iraq. It extends NW–SE for ~17 km within the high folded zone of the northwestern segment of the Zagros Foreland Fold Thrust Belt. The aim of this work is for unraveling the tectonic history and detecting tectonic episodes responded for the initiation and development of the anticlinal structure. More than 450 fracture planes were classified into sets and systems according to their relations with three mutually perpendicular geometric axes (tectonic axes). Tension sets are ac and bc, the first one formed by extension along fold axis accompanying direct compression perpendicular to fold trend, whereas the second is the product of relaxation that motivated the primary compression. The shear systems are hk0, h0l and 0kl developed successively during direct compression and subsequent relaxation episodes of each tectonic force. Field observations and paleostress analysis indicate that the area was subjected to four stress phases. First is primary compressive tectonic phase in the directions NE–SW. The second compressive tectonic stress in the direction NW–SE considered as a secondary phase. Third was extension tectonic phase in the direction NE–SW which developed during the final uplift stage of folding is normal to the major fold trend. The fourth is NW–SE extension face considerate as extension stress related to the primary NE–SW compressive stress.

Keywords: Kalosh anticline, paleostress analysis, fractures analysis, Kurdistan region, Iraq, Zagros

DOI: 10.1134/S0016852120060035

INTRODUCTION

The rock volume is like a tape recorder that is always running. The deformation path is recorded as features in the rock volume, including fractures, folds, and penetrative deformation. Paleostress analysis is the science of reading that tape and determining the deformation path. The deformation path is a powerful technique to provide additional constraint on structural interpretations [14]. Deformation structures that can be observed directly in individual outcrops or with hand specimen are commonly referred to as minor structures or mesostructures such as fractures, stylolites, striated fault planes, veins arrays and brittle shear zones. They nevertheless underpin many structural interpretations. They are the building blocks that allow to understanding of larger scale structures. In structural and tectonic studies these minor structures become widely known because they can be interpreted more accurately [18, 20]. The same approaches and methods cannot be used for studying both small and large structures, for example small faults, and sometimes those of an intermediate size, can be observed and studied at outcrops scale or hundreds of meters in scale. On the other hand, large structures are mainly studied using geological maps prepared from field studies and also from geophysical investigations or from interpretation of aerial photographs or satellite images [8]. Tension fracture is defined as a natural mode I rock fracture [10, 15, 17]. The plane of a propagating fracture is always perpendicular to the local least principal stress that prevailed during fracture propagation. The shear fractures form in undamaged rock initiate as conjugate sets that are oriented parallel to the intermediate stress axis and are generally ±2° to 30° from the maximum stress axis.

Fractures analysis carried out throughout traverses across Kalosh anticline. The anticline is located ~30 km south of Sulaimani city, Kurdistan region northeast Iraq (Fig. 1) [21]. It extends NW–SE for ~17 km within the high folded zone of the western segment of the Zagros Foreland Fold Thrust Belt. It lies between longitudes (44°25′44″ E and 44°33′52″ E) and latitudes

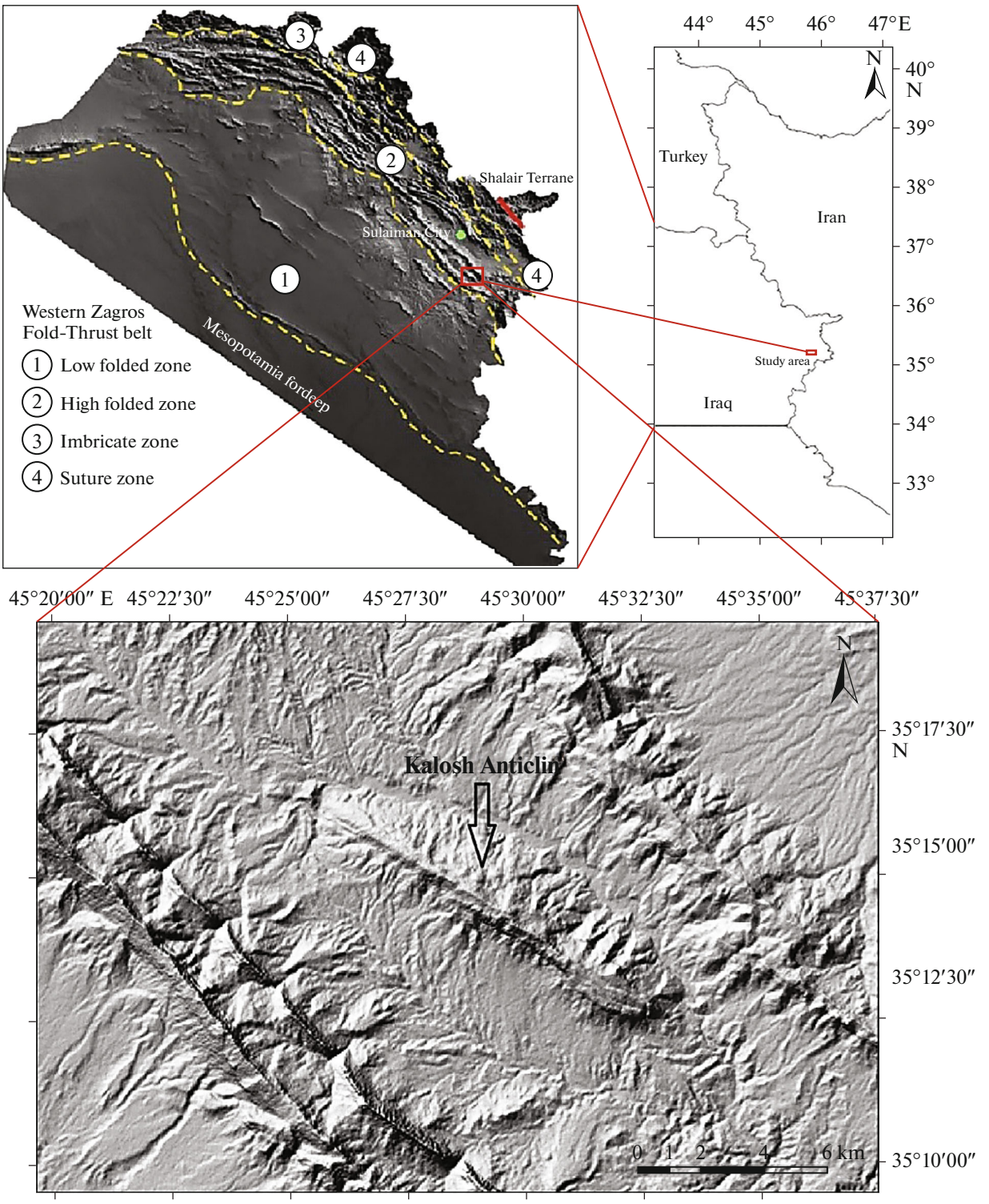

Fig. 1. Location of the study area. The tectonic subdivisions of the Western Zagros Fold–Thrust Belt [12] overlaying digital elevation model of ALOS PALSAR [22].

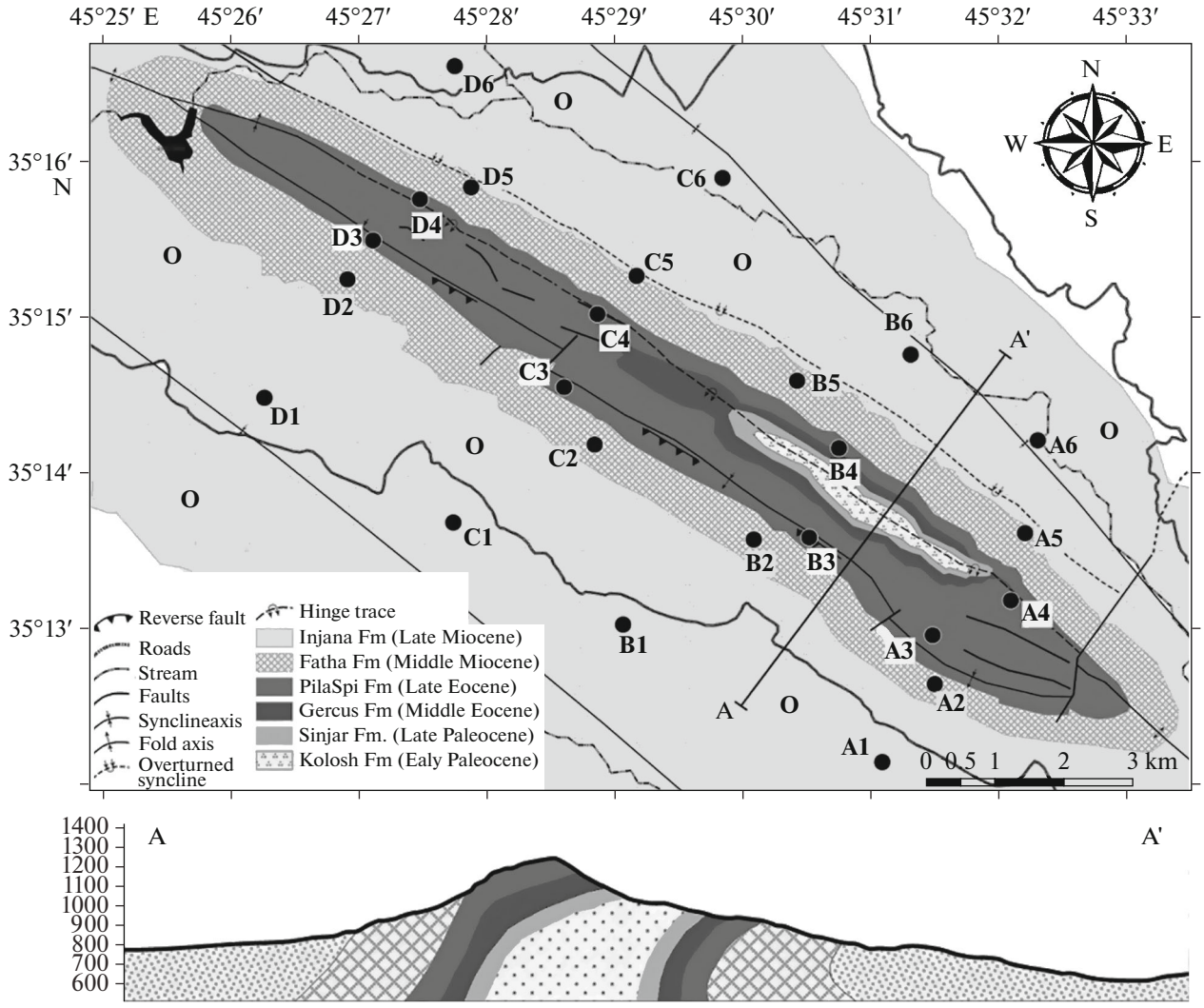

Fig. 2. Geological map and cross section (A–A¯). A, B, C and D, are fracure stations along four traverses of Kalosh anticline.

(35°512′09″ N and 36°16′13″ N). The area is extremely rugged mountainous with high amplitude anticlines.

STRATIGRAPHIC SUCCESSIONS

The stratigraphic successions of the studied area are dominated by the exposures of Tertiary rocks [9] (Fig. 2). During this time, thick clastic unit was deposited in a flysch marginal, narrow NW–SE trending trough Kolosh Formation [5]. Followed by shallow marine carbonate or mixed siliciclastic and carbonate Sinjar Formation of Early Eocene age. Then thick clastic unit was superimposed by red clastic molasses sequence of Gercus Formation of Middle Eocene age. This former molasse trough became a slightly subsiding, partly lagoonal, the basin filled in with the carbonates of the Pila Spi Formation of Middle-Late Eocene, [16]. They followed by thick evaporates, carbonate and marls of the Fatha Formation of Middle Miocene age [6], followed by the deltaic-pedimentary clastics which commence with red silts and marls of Injana Formation that belongs to Upper Miocene [4].

DATA AND METHODS

The fieldwork carried out through 24 stations distributed in the study area along the four traverses. The stations were selected far from plunging area to avoid the tectonic axes rotation and give the most realistic results (Fig. 2). All measurements and results are in Right Hand Rule (RHR). The measurements included the attitudes of bedding and fracture planes.

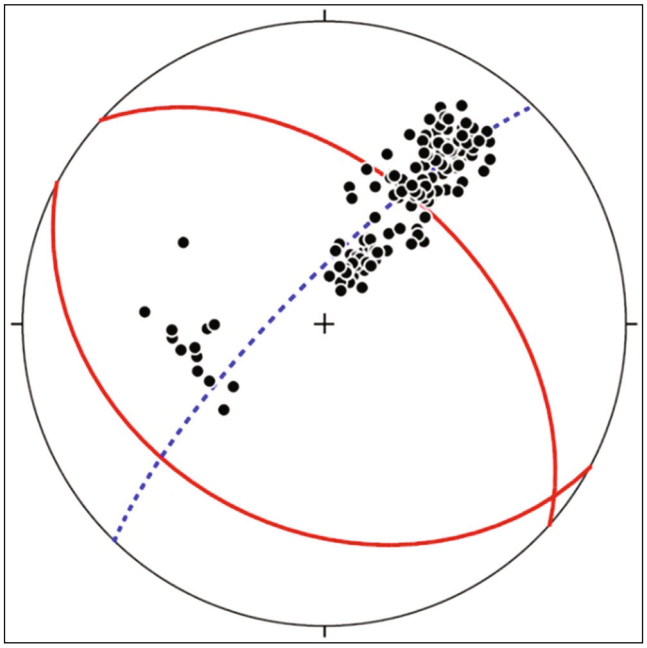

Fig. 3. Synoptic pai diagram of the Kalosh anticline along cross section (A–A¯).

The fracture planes data analyzed stereographically using Dips software (Dips.v5) [21]. The results of fracture analysis were classified according to [13].

Win-Tensor program version 5-8-1 used for determines the paleostress directions (σ_1, σ_2, and σ_3) from the average attitudes of the conjugate shear fracture planes. σ_1 bisect acute angle between conjugate shear fracture planes, σ_3 is perpendicular to σ_1 and bisect obtuse angle, and σ_2 represent the line of the intersection between the two fracture planes [7]. The tension fractures are always perpendicular to the least principal stress (σ_3) and parallel to the maximum stress direction (σ_1).

Finally, the output of the kinematic analyses of structural mode (fractures) unified to conclude the sequence of tectonic phases, which architecture the study area in the view of geotectonic setting of the studied area.

RESULTS

Geometry of the Fold

We studied the geometry of Kalosh anticline through four traverses perpendicular to its axis. These traverses show that the anticline follows the general Zagros fold trend NW–SE, and the anticline is asymmetrical double plunge box fold. It consists of the crestal segment bounded by two limbs. The southwestern limb is slightly steeper while the northeastern limb is overturned. Figure 3 shows the synoptic stereographic pi-diagram of Kalosh anticline along cross section (A–A¯). It shows that the anticline has two hinges. In the SW fold, the attitude of the axial plane is 042°/48°, the attitude of the fold axis is 126°/06°, the average attitude for the northeastern limbs is 202°/22°, the southwestern limb is 210°/63°, the interlimb angle is 138° and the anticline is gentle according to [20]. In the NE fold, the attitude of the axial plane is 208°/33°, the attitude of the fold axis is 124°/04°, the average attitude for the northeastern limbs is 203°/44°, the southwestern limb is 202°/22°, the Interlimb angle is 23° and the anticline is tight according to Fleuty classification [11].

Fractures Analysis

More than (450) readings of fractur planes were collected from 24 stations along four traverses (Fig. 3). Strike and dip were measured for the fracture planes as well as the attitude of the bedding plane, which contain the fracturs. Many of collected data were neglected due to the nonexistence of the two conjugate fractures of the system in the same station.

The stereographic projections of the fracture poles in the all 24 stations are shown in the (Figs. 4, 5). The paleostress analysis for all the 24 stations shown in the (Supplements 1, 2, 3 and 4). All data with paleostress classification are listed in Table 1.

DISCUSSION

From the fracture analysis and classification, two orthogonal tension fracture sets ac and bc together with following shear systems (hk0) acute about (a), (hk0) acute about (b), h0l acute about (a), h0l acute about (c) and 0kl acute about (c) where distinguished in the study area. It is clear from table 1 that the most prevalent paleostress directions are NE–SW and NW–SE. The first NE–SW compressive stress normal to the general trend of the major anticline is considerate as horizontal primary component of oblique collision between Arabian and Eurasian plates. This compressive phase led to initiation (ac) tension set, (hk0) acute about (a) and (h0l) acute about (a). (bc) tension set, and (hk0) acute about (b) indicate that they formed by other compressive stress in the direction NW–SE parallel to sub parallel to the axes of the major fold. This stress considered as secondary stress developed during relaxation event after primary compressive stress. The (hk0) acute about (a) tectonic axis is one of the most prevalent shear fractures in the study area. The approximately (h0l) acute about (c) and (0kl) acute about (c) shear fractures indicate that these fractures may be developed by the extensional

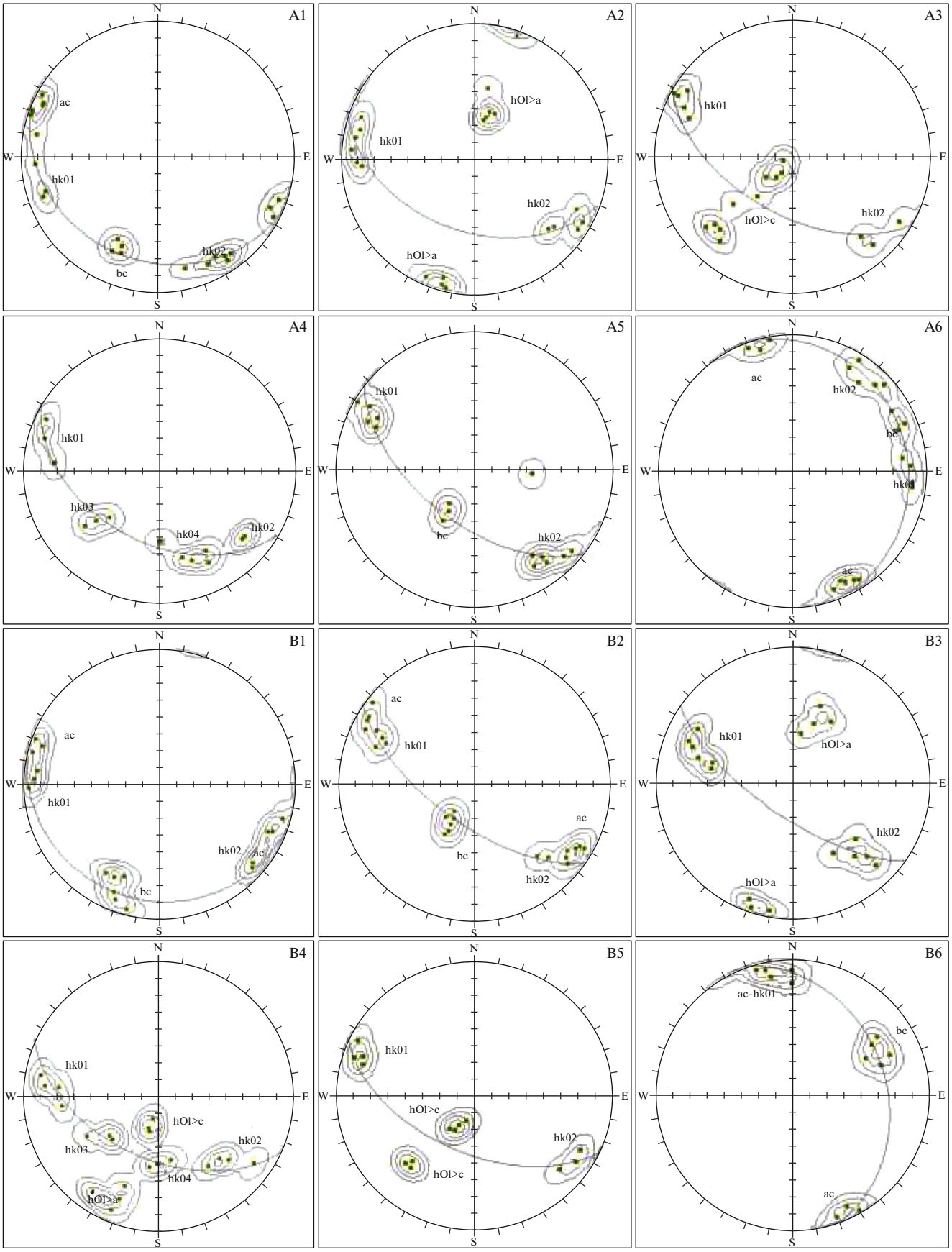

Fig. 4. Pole projections (fractures) and classification for the stations on traverses A and B.

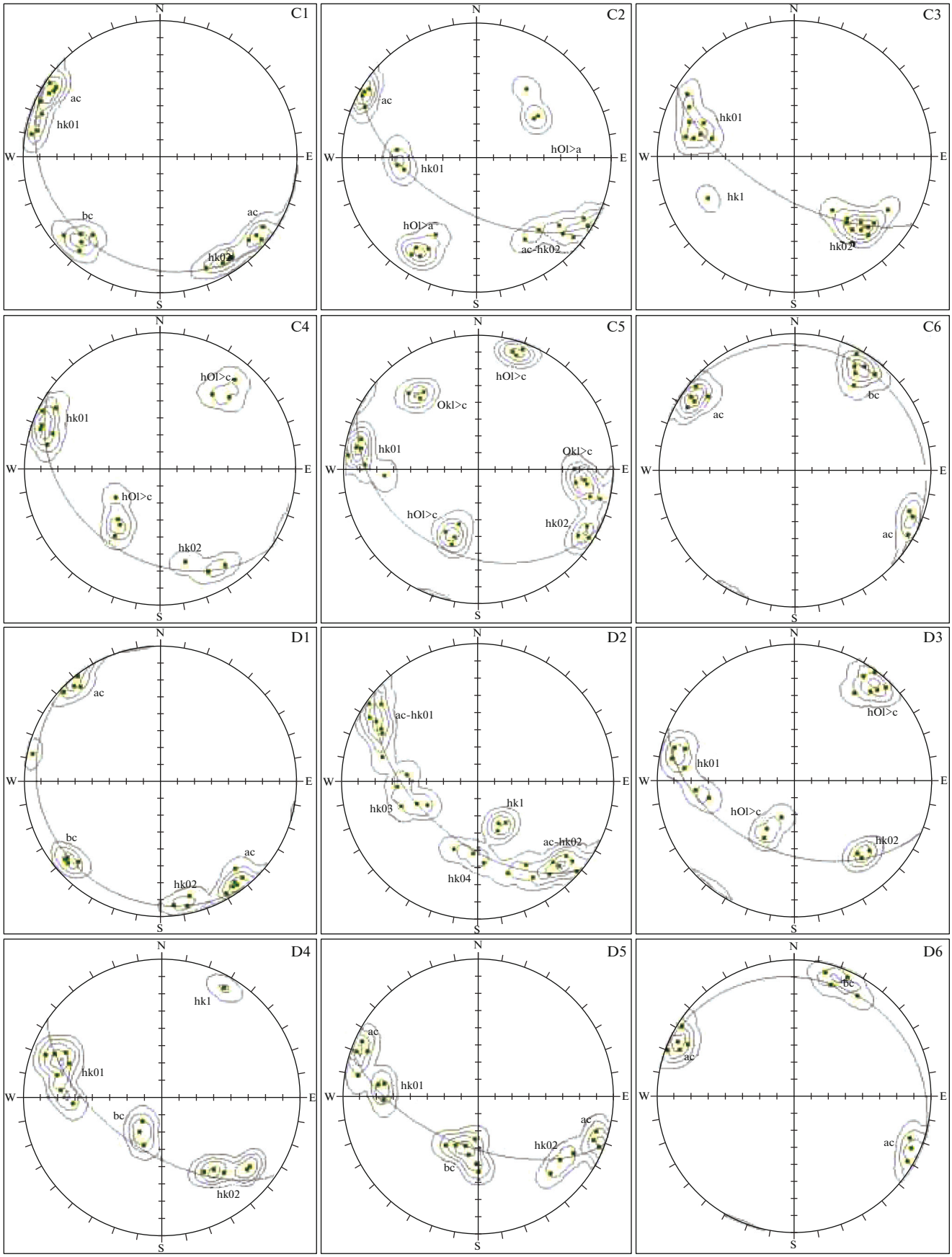

Fig. 5. Pole projections (fractures) and classification for the stations on traverses C and D.

Table 1. Fracture types and paleostress analysis for all 24 stations in the study area

Station	Bedding	Type of fractures	Average attitude of the conjugate fracture planes		Paleostress analysis			Stress direction	Type off stress
					σ_1	σ_2	σ_3		
A1	115/24	ac	020/86	205/80	00/000	00/000	03/112	NW–SE	Tension
		bc	290/60	–	00/000	00/000	30/200	NE–SW	Tension
		hkO > a	356/78	240/74	25/209	65/024	02/188	NE–SW	Compressive
A6	338/15	ac	075/80	244/86	00/000	00/000	03/339	NW–SE	Tension
		bc	160/74	–	00/000	00/000	16/070	NE–SW	Tension
		hkO > b	136/76	178/78	03/336	76/235	14/067	NW–SE	Compressive
A2	110/45	hkO > a	004/80	220/68	42/207	47/015	06/111	NE–SW	Compressive
		hOl > a	284/86	110/30	62/188	03/284	28/016	NE–SW	Compressive
A5	128/58	bc	300/30	–	00/000	00/000	60/210	NE–SW	Tension
		hkO > a	024/72	232/44	66/250	19/031	14/126	NE–SW	Compressive
A3	120/55	hkO > a	228/76	024/74	52/215	38/037	01/306	NE–SW	Compressive
		hOl > c	306/14	314/68	41/047	02/315	49/222	NE–SW	Tension
A4	126/45	hkO > a	220/80	016/76	46/206	44/030	02/298	NE–SW	Compressive
		hkO > b	320/50	250/62	11/291	49/033	39/192	NW–SE	Compressive
B1	110/15	ac	020/85	203/84	00/000	00/000	00/111	NW–SE	Tension
		bc	292/75	–	00/000	00/000	15/202	NE–SW	Tension
		hkO > a	002/80	220/84	23/200	67/026	02/291	NE–SW	Compressive
B6	340/32	ac	078/82	244/84	00/000	00/000	01/341	NW–SE	Tension
		bc	154/62	–	00/000	00/000	28/064	NE–SW	Tension
		hkO > a	090/70	0	0	0	0	NE–SW	Compressive
B2	125/66	ac	026/78	203/84	00/000	00/000	03/294	NW–SE	Tension
		bc	298/32	–	00/000	00/000	58/208	NE–SW	Tension
		hkO > a	224/66	026/64	71/212	19/035	01/305	NE–SW	Compressive
B5	116/55	hkO > a	020/74	214/78	64/203	26/028	02/297	NE–SW	Compressive
		hOl > c	296/20	312/56	36/052	07/317	52/217	NE–SW	Tension
B3	125/70	hkO > a	015/60	225/66	63/204	27/032	03/300	NE–SW	Compressive
		hOl > a	288/66	110/38	76/195	01/289	14/019	NE–SW	Compressive
B4	115/52	hkO > a	222/60	005/62	60/205	30/022	01/113	NE–SW	Compressive
		hKO > b	320/38	270/42	05/300	37/034	53/204	NW–SE	Compressive
		hOl > c	285/20	290/70	45/023	02/291	24/199	NE–SW	Tension
C1	125/20	ac	220/80	032/82	00/000	00/000	01/126	NW–SE	Tension
		bc	312/74	–	00/000	00/000	16/222	NE–SW	Tension
		hkO > a	240/80	012/84	19/217	71/030	02/126	NE–SW	Compressive
C6	300/10	ac	035/82	202/88	00/000	00/000	03/298	NW–SE	Tension

Table 1. (Contd.)

		bc	120/76	–	00/000	00/000	14/030	NE–SW	Tension
C2	120/57	ac	030/86	212/80	00/000	00/000	03/121	NW–SE	Tension
		hkO > a	354/50	222/74	52/184	35/030	13/291	NE–SW	Compressive
		hOl > a	304/70	145/45	71/178	13/312	13/045	NE–SW	Compressive
C5	115/35	hkO >a	214/78	010/76	48/201	42/023	01/292	NE–SW	Compressive
		hOl > c	106/80	290/45	72/006	04/107	18/107	NE–SW	Compressive
		Okl > c	050/58	188/70	53/036	36/204	06/298	NE–SW	Tension
C3	120/65	hkO > a	018/70	228/62	60/220	30/031	04/123	NE–SW	Compressive
C4	125/34	hkO > a	020/82	245/72	31/225	58/034	05/132	NE–SW	Compressive
		hOl > c	134/62	310/40	79/053	02/312	11/222	NE–SW	Tension
D1	140/13	ac	048/84	234/80	00/000	00/000	02/141	NW–SE	Tension
		bc	320/78	–	00/000	00/000	12/230	NE–SW	Tension
		hkO > a	258/80	012/85	14/226	76/033	03/135	NE–SW	Compressive
D6	310/15	ac	025/83	204/86	00/000	00/000	07/295	NW–SE	Tension
		bc	114/80	–	00/000	00/000	10/024	NE–SW	Tension
D2	130/54	ac	035/86	220/80	00/000	00/000	03/127	NW–SE	Tension
		hkO > a	240/70	026/68	53/222	37/044	01/313	NE–SW	Compressive
		hkO > b	274/44	340/40	30/310	37/043	53/216	NW–SE	Compressive
D5	120/60	ac	020/86	202/78	00/000	00/000	04/290	NW–SE	Tension
		bc	285/30	–	00/000	00/000	60/195	NE–SW	Tension
		hkO > a	217/65	008/60	64/197	26/024	03/293	NE–SW	Compressive
D3	124/58	bc	302/24	–	00/000	00/000	66/212	NE–SW	Tension
		hkO > a	230/60	012/66	57/215	33/028	03/120	NE–SW	Compressive
D4	112/45	hkO >a	230/64	006/70	49/210	41/024	03/117	NE–SW	Compressive
		hOl > c	300/34	132/78	67/058	07/311	22/218	NE–SW	Tension

phase associated with NE–SW and NW–SE compressive stresses (Fig. 6).

The clockwise rotation of the NNE–SSW paleostress direction to the NE–SW which is perpendicular to sub-perpendicular to the general trend of the anticline with the following direction of maximum stress (σ_1) (52°/184°) and (66°/250°) might be attributed to the oblique collision of the Arabian and Eurasian plates along their zigzag margins (Fig. 7).

The combination of the above fractures, which analyzed to find the direction of maximum principal stress revealed that the anticline formed by the NE–SW stress direction then developed by the uplifting process that make it to crestal extension in which the anticline changed from the symmetrical box fold to overturned NE vergence.

This two main compressional paleostress directions NE–SW and NW–SE, which are resulted from the fracture analysis for the study area, also mentioned by many authors who have investigated paleostress in different areas of north and northeast of Iraq such as; [1–3, 19].

CONCLUSIONS

(1) Paleostress analysis from fractures indicated that the study area was subjected to four stress states. Two of them are compression, and the rest two are extensions.

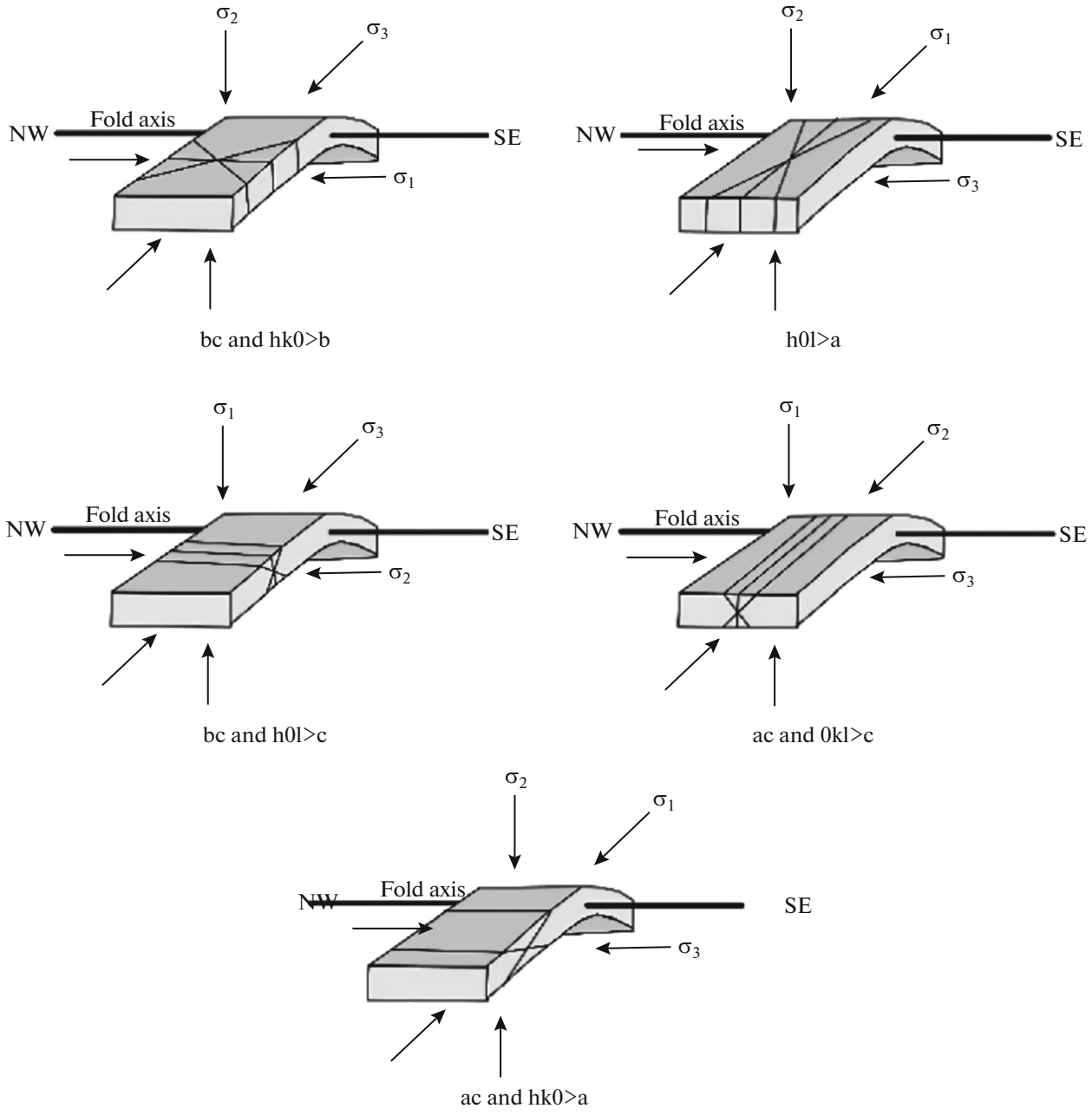

Fig. 6. Relation between fractures set and systems with the stress directions in Kalosh anticline.

(2) The primary stress is the compressive stress with their maximum horizontal axis (σ_1) in the direction of NE–SW, seams as responsible to the initial folding and most of the brittle failures in the area.

(3) The NW–SE compressive stress is parallel to sub-parallel of the fold axis, considered as secondary stress developed during the relaxation event succeeding the primary compressive pulse. This stress is responsible for the other brittle failures in the area.

(4) The NE–SW extension stress considered as a releasing phase that associated with the final uplift of the main fold.

(5) The NW–SE extension face considerate as an extension stress related to the primary NE–SW compressive stress.

(6) The clockwise rotation of the NNE–SSW paleostress direction to the NE–SW it might be attributed to the oblique collision of the Arabian and Eurasian plates along their zigzag margins.

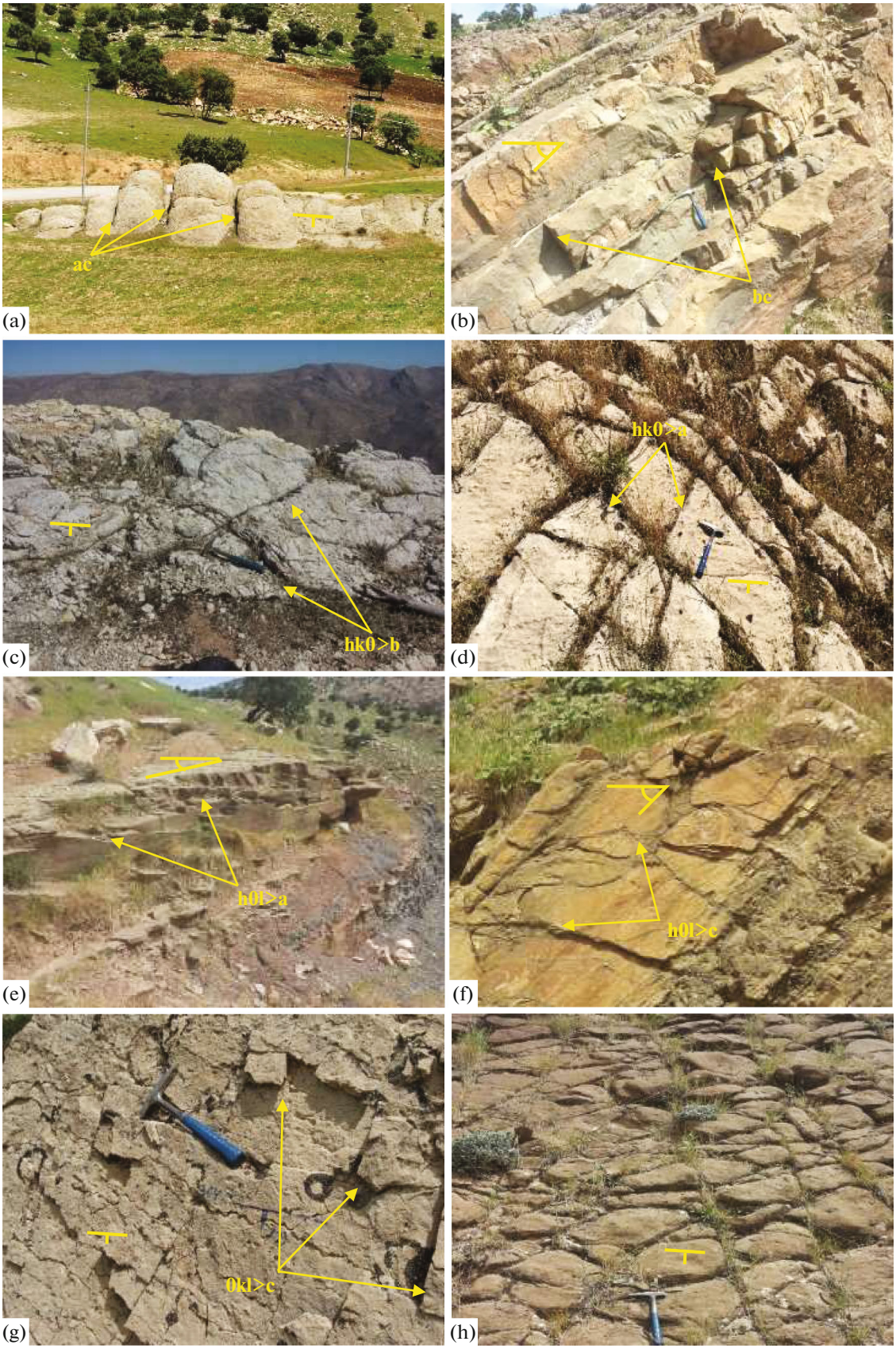

Fig. 7. Different types of fractures in the study area.

ACKNOWLEDGMENTS

We are grateful to Dr. Ahmed K. Obaid (University of Baghdad, Iraq) and Dr. Arsalan A. Othman (Iraqi Geological Survey, Iraq) for their help and consulting that improved the manuscript.

SUPPLEMENTARY MATERIALS

Supplementary materials are available for this article at doi: 10.1134/S0016852120060035 and are accessible for authorized users.

REFERENCES

1. H. G. M. Adeeb and I. S. I. Al-Jumaily, "Mesofracture analysis of Azmur Anticline, North Eastern Iraq," Iraqi Nat. J. Earth Sci. **10**, 1–24 (2010).
2. I. Al-Fadhli, Y. Janardan Rao, G. Oweiss, and M. Khalil, "Polyphase deformation in apart of Zagros, Sulaimaniyah district, NE Iraq," J. Indian Acad. Geosci. **22**, 1–31 (1979).
3. S. H. S. Al-Hakari, "Paleostress analysis from brittle failure and minor structures in Dokan Area, Kurdistan Region, NE of Iraq," J. Zankoy Sulaimani, Pt. A. **18**, 283–310 (2017).
4. A. I. A. Al-Juboury, "The Upper Miocene Injana (Upper Fars) formation of Iraq: Insights on provenance history," Arab. J. Geosci. **2**, 337–364 (2009).
5. S. K. Al-Shaibani, B. A. Al-Qayim, and L. Salman, "Stratigraphic analysis of Tertiary–Cretaceous contact, Dokan area, North Iraq," J. Geol. Soc. Iraq. **19** (2), 1–26 (1986).
6. B. M. Ameen, "Sequence stratigraphy of Gercus Formation (Middle Eocene) in Sulaimaniya Area, Northeastern Iraq," Iraqi Natl. J. Earth Sci. **6** (2), 23–32 (2006).
7. E. M. Anderson, *The Dynamics of Faulting and Dyke Formation with Applications to Britain* (Oliver & Boyd, Edinburgh, 1942).
8. J.-L. Blès and B. Feuga, *The Fracture of Rocks* (North Oxford Academic, Oxford, 1986).
9. T. Buday, *The Regional Geology of Iraq: Stratigraphy and Paleogeography*, Ed. by Dar Al-Kuttib (Univ. Mosul, Mosul, Iraq, 1980).
10. T. Engelder, "Analysis of pinnate joints in the Mount Desert Island granite: Implications for postintrusion kinematics in the coastal volcanic belt, Maine," Geology **17**, 564–567 (1989).
11. M. J. Fleuty, "The description of folds," Proc. Geol. Assoc. **75**, 461–492 (1964).
12. S. F. Fouad, "Western Zagros fold–thrust belt, part II: The high folded zone," Iraqi Bull. Geol. Min. **6**, 53–71 (2014).
13. P. L. Hancock and M. S. Atiya, "Tectonic significance of mesofracture systems associated with the Lebanese segment of the Dead Sea transform fault," J. Struct. Geol. **1**, 143–153 (1979).
14. A. Lacazette, "Paleostress analysis from image logs using pinnate joints as slip indicators," AAPG Bull. **93**, 1489–1501 (2009).
15. L. B. Thompson, "Natural fracture nomenclature," in *Atlas of Borehole Imagery*, No. 13 of *AAPG Discovery Ser.*, 2nd ed (2009).
16. F. A. Lawa, PhD Thesis (Sulaimani, Iraq, 2004).
17. D. D. Pollard and A. Aydin, "Progress in understanding jointing over the past century," Geol. Soc. Am. Bull. **100**, 1181–1204 (1988).
18. J. G. Ramsay and M. I. Huber, *The Techniques of Modern Structural Geology*, Vol. 2: *Folds and Fractures* (Academic, London, 1987).
19. M. A. Taha, S. N. Al-Saadi, and I. S. Ibrahim, "Microtectonic study Dokan area NE Iraq," Iraqi Geol. Soc. J. **28** (1), 25–35 (1995).
20. B. A. vand der Pluijm and S. Marshak, *Earth Structure: An Introduction to Structural Geology and Tectonics*, 2nd ed. (WW Norton, New York, 2004).
21. Dips 5.1. https://www.rocscience.com/software/dips. Accessed March 24, 2019.
22. Capture date September 9, 2015. https://vertex.daac.asf.alaska.edu/. Accessed November 17, 2015.